Journal of Applied Science and Engineering, Vol. 18, No. 3, pp. 0–0 (2015) *DOI: 10.6180/jase.2015.18.3.??*

Confluent Thermal Lesion Formation in Liver with Radio Frequency Ablation by Using Internally Cooled Multiple-Electrode Technique: Computational Results

Huang-Wen Huang

Department of Innovative Information and Technology, Langyang Campus, Tamkang University, Tamsui, Taiwan 251, R.O.C.

Abstract

Radiofrequency ablation (RFA) has been used successfully in the treatment of liver tumors. However, current RFA procedures are less effective against tumors that are large. The purpose of this study was to investigate internally cooled multiple-electrode technique with radio-frequency ablation (RFA) which technique could provide larger thermal lesion by using computer simulation and to determine optimal RF electrode spacing based on coagulation necrosis zone volume. Multiple electrically independent electrodes have been powering up by switching to the next electrode at a predetermined time interval of certain time period. As to computer models, the mathematical equations use Laplace equation of electric field calculation, and Bio-heat transfer equation of calculation temperature field. Numerical methods will consider Gauss-Seidel iteration to obtain 3-D finite difference solutions of a set of partial differential equations for a simple three-dimensional cubic geometry model. Maximum tissue temperature ($T_{\max}$) is used as a critical index for reaching thermal lesion formation during RFA and threshold temperature (T_{thresh}) is used to estimate coagulation zone volume. Cylindrical RF cool-tip electrode is internally cooled at constant water temperature. Results showed several clover-shaped resultant coagulation necrosis and enlarged thermal lesions which were consistent with experimental results.

***Key Words*:** Multiple-electrode, Internally-cooled Electrode, Radiofrequency Ablation, Coagulation Necrosis, Bio-heat Transfer

1. Introduction

Radiofrequency ablation (RFA) is a minimum invasive and localized treatment designed to destroy tumors by heating tissue to temperatures that exceed 55 °C. It has received increased attention as an effective minimally invasive approach for the treatment of patients with a variety of primary and secondary malignant neoplasms [1]. The coagulation necrosis threshold temperature varied and it normally is based on experimental observations. Some stated it is 60 °C [2] and no coagulation was seen when local temperature was less than 50 °C [3]. Thermal ablations require higher temperatures in the treated volume than hyperthermia which is a term normally regarded as treating temperatures ranging from 41 °C to 45 °C with a period of 30~60 minutes. For ablations, it takes less time to denaturalize proteins within a matter of 4~6 minutes. As RFA has been successfully in the treatments of tumors of liver, lung, bone, breast, and kidney [4–7], at present, RFA is more commonly employed than other local ablative modalities in Taiwan because the technique is highly effective, minimally invasive, and requires fewer sessions. However, current RFA procedures are less effective against tumors that are large [8]. Many research groups stated RFA is effective for small and favorably situated tumors, but local progression rates are substantially higher for large tumors ($\geqq$ 4-cm) [9,10]. Many factors contribute to high post-radiofrequency local re-

*Corresponding author. E-mail: hhw402@mail.tku.edu.tw

currence rates, but the in-ability of single-electrode RF systems to create adequately large zones of ablation has been crucial. The large coagulation zone volume requires overlapping ablations to treat moderately sized tumors [11].

The overlapping ablations can produce large zone of necrosis, but the multi-electrode ablation technique requires the treating configuration which is time consuming [12]. The configuration should avoid damaging vital organs nearby the treated tumor region. Thus the computer simulations provide a fast and better analysis to design an optimal solution, such as locations of RF probes before clinical RFA treatments. As to the key to overlapping ablations for multi-electrode RFA is power control. The switching system is an addition to the base generator (which is normally for single electrode system) and is capable of powering up to three electrically independent electrodes by switching to the next electrode once the impedance reaches 30 Ω above the baseline or at a predetermined time interval of 30 seconds [12–14].

About computer models, most numerical programs used commercial programs of finite element methods (FEM) [15,16] to do pre-treatment analysis, particular to monopolar and bipolar ablation with 4-prong probe (RITA model 30) [17]. The monopolar model with hooked electrodes shows a mushroom shaped lesion. Some early finite element models [18–20] of RFA focused on catheter ablation in the treatment of cardiac arrhythmias [21]. Some developed FEM models are interested in hepatic ablation using single electrode without internally water cooling effect [22,23]. In comparisons with FEM, the finite difference method (FDM) model has not been found many due to its difficulty to handle irregular geometry. However FDM can execute sophisticated calculations efficiently in rather simple geometry. Recently Huang [24] used finite difference methods to illustrate thermal lesion formation of the impact of blood vessel during RFA. His FDM model has been successfully tested in hyperthermia treatments with the impact of thermally significant blood vessels [25,26].

The objective of this study is to illustrate the capability of multi-electrode RFA technique to generate large confluent thermal lesion formation during liver tumor treatments by using computer simulation. The overlapping thermal lesion effect will be demonstrated. Extreme high thermal gradients near the internally-cooled electrode is captured numerically and presented. In comparison with experimental results, the calculated coagulation necrosis zone volume by single-electrode RFA is in a good agreement with experimental results [14]. For three-electrode RFA case of computational results, the clover-shape thermal lesion formation is graphically shown, and it is consistent with the three-electrode experimental results (Figure 1 of reference [13]).

2. Methods

2.1 Formulation of the Problem

The computer model was set up to investigate the present study. Figure 1(a) showed a cubic geometry with dimensions: 80-mm by 80-mm by 80-mm in (W, D and H) illustrating the computational domain of the study. Within the domain, three internally-cooled electrodes have inserted along the z-direction, with active-tip exposures

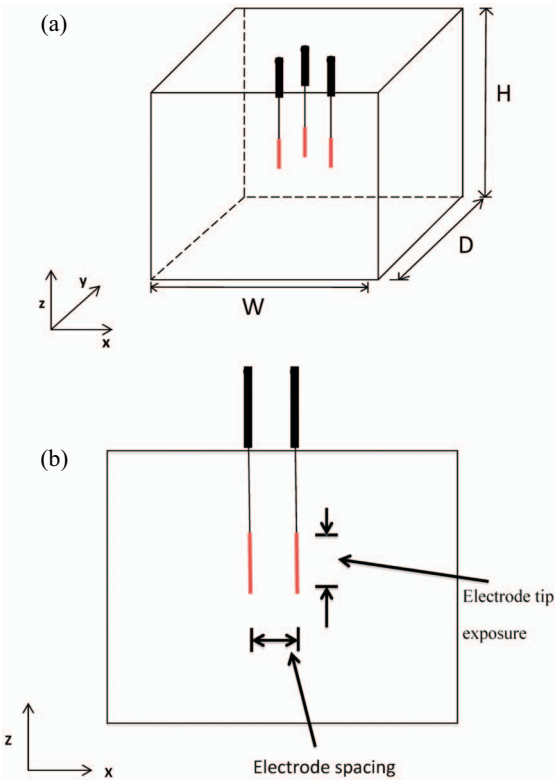

Figure 1. (a) A cubic geometry with dimensions 80-mm by 80-mm by 80-mm in (W, D and H) illustrating the computational domain of study. Within the domain three internally-cooled electrodes have inserted along z-direction into the center of the domain. (b) The central x-z plane illustrating two internally-cooled electrodes along z-direction with same electrode tip exposure length, the two electrodes have an electrode spacing between them.

into the central area of the domain. Figure 1(b) showed the central x-z plane illustrating two internally-cooled electrodes along the z-direction with same electrode tip exposure length, and the two electrodes have electrode spacing between them. The computational domain is designed to be sufficiently large to capture the local heat treatment of RF electrodes at the center.

The single cylindrical Radiofrequency (RF) cool-tip electrode is placed at the center of the cube, with a 1.5-mm in diameter and a length of possible 1.0, 2.0 and 3.0-cm exposure in the z-direction. RF electrode's material properties and electrical conductivity are set according to Tungjitkusolmun's paper [27]. One of the commercially available systems is the Radionics Cool-Tip system (Radionics, Burlington, MA). This system uses 17-gauge (with a diameter of 1.5 mm) RF electrodes with active tip exposures of 1, 2, and 3 cm. Covidien (ValleyLab Co. Boulder, Colorado) offers the electrodes in their Cool-tip™ RF system [28] as well. The blood perfusion rate is uniformly distributed in the domain. To well capture multiple-electrode overlapping thermal impacts, the electrodes run in the z-direction which is parallel to the z-axis in the studies. And, the electrodes' active tip exposures located at the center area of the domain, generated electrical flow out to the dispersive ground pad (0 V) at the outer domain boundaries through resistive tissue media. The flow chart of computational model is shown in Figure 2. A detailed description of the maximum temperature index (T_{max}), which is another form of setting power density in RFA will be described in section 2.3. And, the threshold temperature is used to estimate the coagulation necrosis zone volume described in section 2.4.

2.2 Computational Flow Chart and Power Scheme Under RFA

The computational flow for RF ablation with single electrode is shown in Figure 2(a). Mathematical partial differential equations were solved to calculate power depositions around RF electrode, and tissue temperatures. Iterative electrical power will be added during heating process (i.e. numerical computation) until T_{max} reached and then thermal lesion formation obtained. For multiple-electrode RFA treatments, a switching controller is needed to power each electrode one at a time with short duration (normally 30 sec [12]). For computational model, an independent RF electrode is assumed for multiple-electrode RF heating configuration system. Overlapping heating zone is formed by adding energy contribution from each electrode in the system. Figure 2(a) showed computational flow chart of calculating thermal

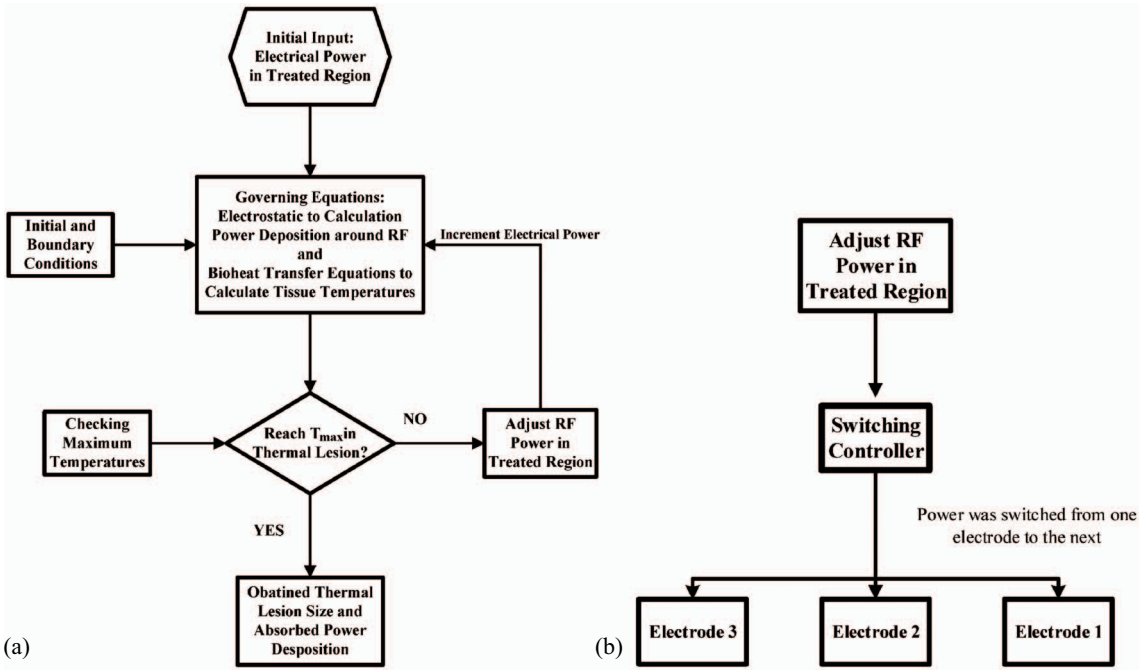

Figure 2. (a) Computational flow chart of calculating thermal lesion formation under single RF heating. (b) Considering multiple-electrode RFA heating process, the additional switching controller is needed to direct electrical power to one RF electrode at a time.

lesion formation under single RF heating. And, Figure 2(b) showed with considering multiple-electrode RFA heating process, the additional switching controller is needed to direct electrical power to one RF electrode at a time. At present, commercial RF system could provide up to three electrodes in thermal ablations.

2.3 Maximum Temperature Heating Limit Indicator ($T_{\max}$)

To limit excessive dissipated power deposition in thermal lesions through electrical current, the maximum temperature heating limit indicator ($T_{\max}$) is introduced in the studies. It represents temperature-controlled heating process. $T_{\max}$ is defined as the temperature is approaching to $T_{\max}$ in thermal lesion, but less than $T_{\max}$ within a small range (i.e. $T_{\max}$ is that the temperature is near but not exceeding $T_{\max}$). That is,

$$T < T_{\max} \tag{1}$$

and

$$\left|T - T_{\max}\right| < \varepsilon \tag{2}$$

where ε is the precision error, and is set to 1.5 °C. The introduction of disturbance is reasonable in computational model. Equations 1 and 2 state that continuous incremental electrical power deposition stopped as any temperature in thermal lesion approximately reached $T_{\max}$ within a ε distance.

2.4. Thermal Lesion Region Boundary Indication (T_{band}) and Thermal Lesion Threshold Temperature (T_{thresh})

To effectively treat the target region and be able to estimate the thermal lesion, visual analyzing thermal lesion plays a significant role in successfully managing RFA treatment. Conventionally, temperatures above 50–54 °C for 4–6 minutes are required to kill cancerous cells during RF heating [29]. To cause tissue cell destruction for RFA by producing heat energy, some thought raising the temperature of tissue to greater than 50 °C–54 °C [30,31]. Some stated the threshold temperature for tissues to be ablated is 60 °C [2]. The threshold temperature, 55 °C, is assumed to kill cancerous cells in the study. To graphically view the thermal lesion in temperature contour plots, a lesion region boundary indicator (T_{band}) (i.e. color band) is used. There are two indicators in contour plots: one is very close to the cool-tip electrode and not easy to detect due to high thermal gradient. The other one locates further away from the electrode and can be easily detected. Here the latter indicator is defined as the following: T_{band} is a temperature band with color in grey, which indicates temperatures in between 55 °C and 60 °C. That is 55 °C $\leqq T_{band} \leqq$ 60 °C. In a simple case without disturbances from blood vessel, the inward boundary of the T_{band} towards the electrode is 60 °C and the other boundary towards the domain boundary is 55 °C as water cooling temperature at electrode remains lower temperature than 37 °C (i.e. 10 °C). The T_{band} indicator assists us in identifying thermal lesion size (i.e. coagulation necrosis zone volume) at present studies.

Additionally, thermal lesion threshold temperature (T_{thresh}) is used in the computer model to estimate coagulation necrosis zone volume. Some argued that the threshold temperature varied with treating duration [29,31]. Since higher temperature ablations require less time to denaturalize protein. Thus, T_{thresh} of 55 °C and 60 °C are chosen to numerically estimate the averaging volume which is checked normally through experimental observation with variations.

2.5 Mathematical Equations for the Electrostatic and Thermal Models

The governing equations under RF heating studies are two models: tissue with blood perfusion model to calculate steady-state temperatures of tissue and the electrostatic field model is to calculate electric power deposition. Since heating temperatures during RFA rise quickly, the steady-state solution is a good approach to view thermal lesion formation [24]. Constant thermal and electrical properties are assumed. First, the electric field is solved and following boundary conditions are set. (a) Ground potential (0 V) at the outer cube boundary. (b) Potential V at the conductor, resulting in constant current density $J(r_0) = J_0$ at the conductor surface ($r = r_0$). From the law of charge preservation, the current at a radius r as a function of the current at the conductor surface, J_0, that is:

$$J(r) = J_0 \times \frac{r_0}{r} \tag{3}$$

And, electrostatic equation is used to calculate dissipated power density (p_e). That is,

$$p_e = J \cdot E = \frac{J^2}{\sigma} = \frac{1}{\sigma}\frac{(J_0 r_0)^2}{r^2} \quad (4)$$

For simplicity to obtain total current, system time-average electrical resistant is assumed constant. As a result, $T_{\max}$ is maximum temperature which is allowed to have continual electrical power added in the system and thus define the thermal lesion size. After obtaining the power p_e, the Pennes bio-heat transfer equation is used to calculate tissue temperatures. That is,

$$\nabla \cdot (k \nabla T(x,y,z)) - \dot{w}_b c_b (T(x,y,z) - T_a) + p_e = 0 \quad (5)$$

where k, c_b, w_b, and p_e are thermal conductivity of soft tissue, specific heat of blood, blood perfusion rate and absorbed thermal power density, respectively. The metabolism effect is neglected in the bio-heat equation due to its limited effect on temperature distribution during heat treatment.

2.6 Numerical Model

The computer model is numerically solved by finite difference method. The numerical scheme used to calculate the temperatures is a black and red finite difference SOR method [32]. It is a robust scheme with convergence and accuracy. And, the numerical scheme to calculate temperatures around and at cylindrical RF probe tip is a one-node approach [33]. The electrical power heating in confluent lesion is by adding up all contributing power from each electrode of the multiple-electrode RFA system. Since each electrode is independent at present system. The numerical details and validation were described by Chen and Huang [33,34]. The thermal resistances around the circular vessels were calculated using the logarithmic resistance approach as described by Chen and Roemer [35]. The property values used in treated tissues are $k = 0.5$ W/m^3/°C, $c = c_b = 4000$ J/kg/°C and $\rho = 1000$ kg/m^3. In all cases, a finite difference nodal spacing of 1-mm is used. Test results with a nodal spacing of 1 mm for test cases using either the arterial vessel network (when no veins are present) or the countercurrent vessel network [36] showed no significant differences with the results of the comparable 2-mm nodal spacing models. The boundary temperature is set to 37 °C at the outer cubic surfaces. The internally-cooled electrode water temperature is kept at constant 10 °C.

3. Results

For simplicity, tumor and normal tissue properties are the same tissue element (Table 1) at present. Material properties used in computational model throughout the studies, unless notified, are described in Table 1. All case studies presented here are to highlight the capability of the simulator in estimating internally-cooled multiple-electrode radiofrequency ablation (RFA) thermal lesion formation, such as impacts of tip exposure length, electrode spacing and different $T_{\max}$. Practical liver blood perfusion rate of 6.4 (kgm^{-3} s^{-1}) [37,38] is used. In all cases unless notified, $T_{\max}$ = 100 °C T_{thresh} = 55 °C and WCT (water cooling temperature) = 10 °C are used.

3.1 A Single Internally-cooled Electrode Case (for an Index of Coagulation Zone Volume Calculation)

Figure 3 showed thermal lesion formation of single internally cooled electrode with 2-cm tip exposure in liver. The active-tip electrode is placed at the center of the computational domain, along the z-direction from z = 3-cm to 5-cm. Figure 3(a) and 3(b) showed temperature distributions of the central x-z plane (i.e. y = 4-cm) and x-y plane (i.e. z = 4-cm), respectively. The grey color band revealed the lesion boundary. With water cooling temperature of 10 °C, the electrode tip exposure is assumed to maintain uniform 10 °C. Cylindrical shape of thermal lesion shown in Figure 3(a) and circular shape of thermal lesion shown in Figure 3(b) represented largest longitudinal and cross-sectional lesions of RFA in liver. They are typical clinical results. The coagulation zone volume of the single electrode RFA is used as an index

Table 1. Material properties used in computational model for electrical conductivity of liver tissue and RF cool-tip electrode

Element	Material	ρ (kg/m^3)	c (J/kg K)	k (W/m K)	σ (S/m) (at 25 °C)
Active RF probe tip (Ref. 27)	Stainless steel	21500	132	71	$4 \cdot 10^6$
Tissue (Ref. 36)	Liver	1000	4000	0.5	0.333
Blood perfusion (Ref. 24,36)	Blood	1000	4000	0.5	0.333

to estimate that of the multiple-electrode RFA.

3.2 Two-electrode Case with Different Electrode Spacing

To present the impact of electrode spacing, the electrode spacing of 1-cm and 2-cm are used to illustrate the lesion formation. Figure 4 showed temperature distributions for two-electrode radiofrequency ablation at different electrode spacing. The electrode tip exposure length is 1-cm. Figures 4(a) and 4(b) showed tempera-

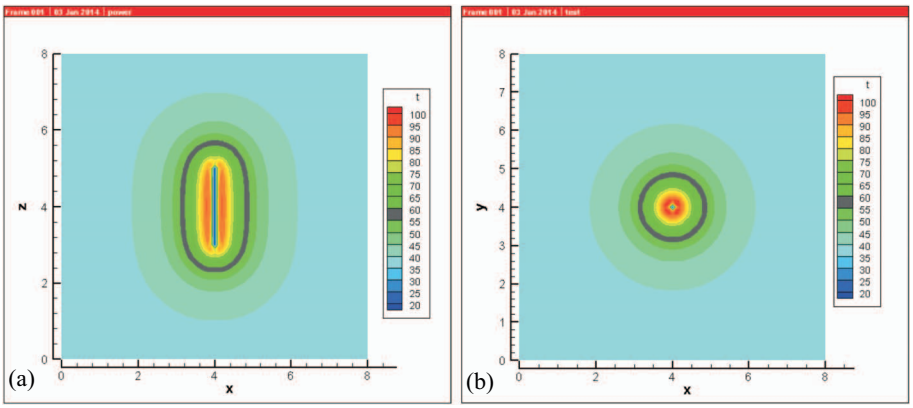

Figure 3. Thermal lesion formation of single internally cooled electrode with 2-cm tip exposure in liver. The electrode is placed at the center of the computational domain, along z-direction from z = 3-cm to 5-cm. (a) Viewing at the central x-z plane (i.e. y = 4-cm). (b) Viewing at the central x-y plane (i.e. z = 4-cm). The grey color band revealed the lesion boundary. With water cooling temperature of 10 °C, the electrode tip exposure is assumed to maintain uniform 10 °C.

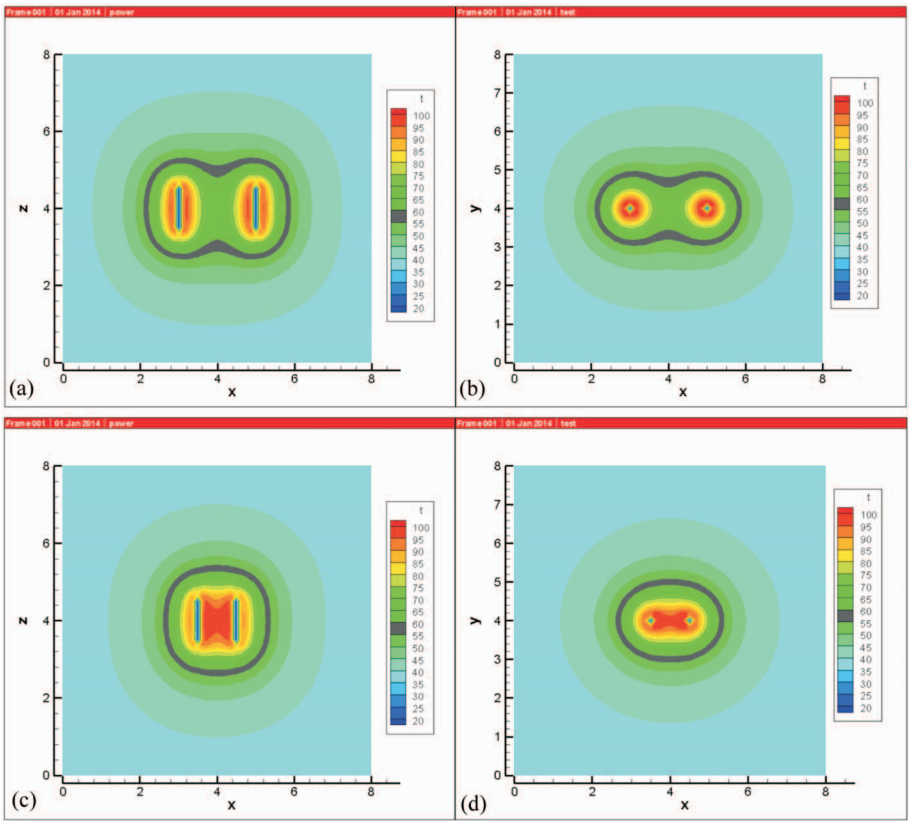

Figure 4. Temperature distributions for two-electrode radiofrequency ablation at different electrode spacing. The electrode tip exposure length is 1-cm. (a) of X-Z and (b) of X-Y planes are at the central planes with the spacing of 2-cm. The internally-water cooled electrodes are placed along z-dir. (c) of X-Z and (d) of X-Y planes at the central planes with the spacing of 1-cm. The internally-water cooled electrodes are placed along z-dir.

ture distributions with the electrode spacing of 2-cm in the central X-Z and X-Y planes, respectively. The internally-water cooled electrodes are placed along z-dir. Figures 4(c) and 4(d) showed temperature distributions with the spacing of 1-cm in the central X-Z and X-Y planes, respectively. When the spacing is 2-cm, the concave shape of T_{band} lesion boundary appeared on the top and bottom of thermal lesion formation on both planes as shown in Figures 4(a) and 4(b). On the other hand, when the spacing is 1-cm, the shapes on the top and bottom, shown in Figure 4(c) and Figure 4(d), are becoming more convex and rounded shape. Further, there is a larger high- temperature zone focused on the center area (which is between two cooled electrodes) of the lesion.

3.3 Two-electrode Case with Different Tip Exposure Length

To understand the impact of tip exposure length, the same conditions shown in Figure 4 have changed only to vary the tip exposure length from 1-cm to 2-cm. Figure 5 showed temperature distributions for two-electrode radiofrequency ablation with the electrode tip exposure length of 2-cm at different electrode spacing. Figure 5(a) of X-Z and Figure 5(b) of X-Y planes show temperature distributions at the central planes with the electrode spacing of 2-cm. The internally-water cooled electrodes are placed along z-dir. Figure 5(c) of X-Z and Figure 5(d) of X-Y planes show temperature distributions at the central planes with the electrode spacing of 2-cm. Both Figures 4(a) versus 5(a), and Figures 4(c) versus 5(c) indicated that the coagulation necrosis zone volume can be significantly impacted by electrode tip exposure length shown in the x-z planes as the length increasing from 1-cm to 2-cm (in the longitudinal direction), regardless of electrode spacing. In latitudinal cross section of electrode figures in x- or y- direction (i.e. Figures 4(b) versus 5(b)), the impact of tip exposure length appeared subtle. A minor increase in coagulation zone volume can be detected.

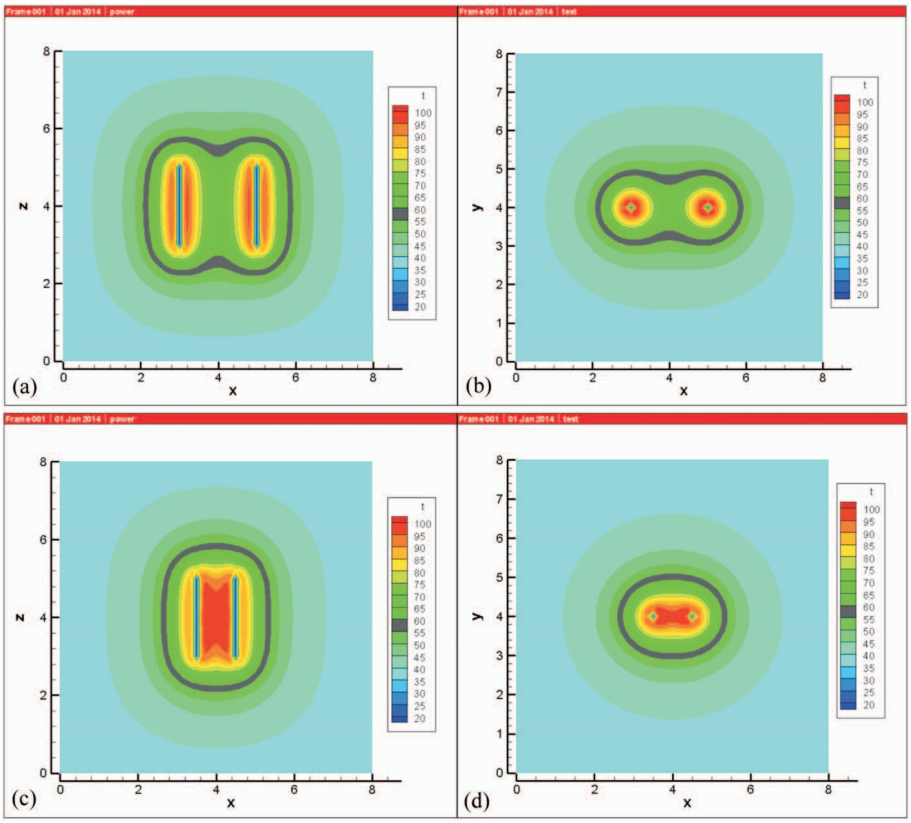

Figure 5. Temperature distributions for two-electrode radiofrequency ablation with the electrode tip exposure length of 2-cm at different electrode spacing. (a) of X-Z and (b) of X-Y planes are at the central planes with the electrode spacing of 2-cm. The internally-water cooled electrodes are placed along z-dir. (c) of X-Z and (d) of X-Y planes are at the central planes with the electrode spacing of 2-cm. The internally-water cooled electrodes are placed along z-dir.

3.4 Two-electrode Case with Different Lesion Maximum Temperatures

During clinical treatments, different maximum temperature in the lesion due to electrical supply may have different lesion formation. Figure 6 showed temperature distributions for two-electrode radiofrequency ablation with the electrode tip exposure length of 2-cm and the electrode spacing of 1-cm at different maximum temperature (T_{max}) in the lesion. Figures 6(a), 6(c) and 6(e) are the central x-z planes illustrating thermal lesion formation at T_{max} = 100 °C, 90 °C and 80 °C respectively. And, Figures 6(b), 6(d) and 6(f) are the central x-y planes illustrating thermal lesion formation at T_{max} = 100 °C, 90 °C and 80 °C respectively. Those figures showed the coagulation zone volume shrank in the decreasing T_{max} from 100 °C to 80 °C as indicated from T_{band} lesion boundary contour in the figures.

3.5 Optimal Solutions

The electrode spacing is considered to be a very im-

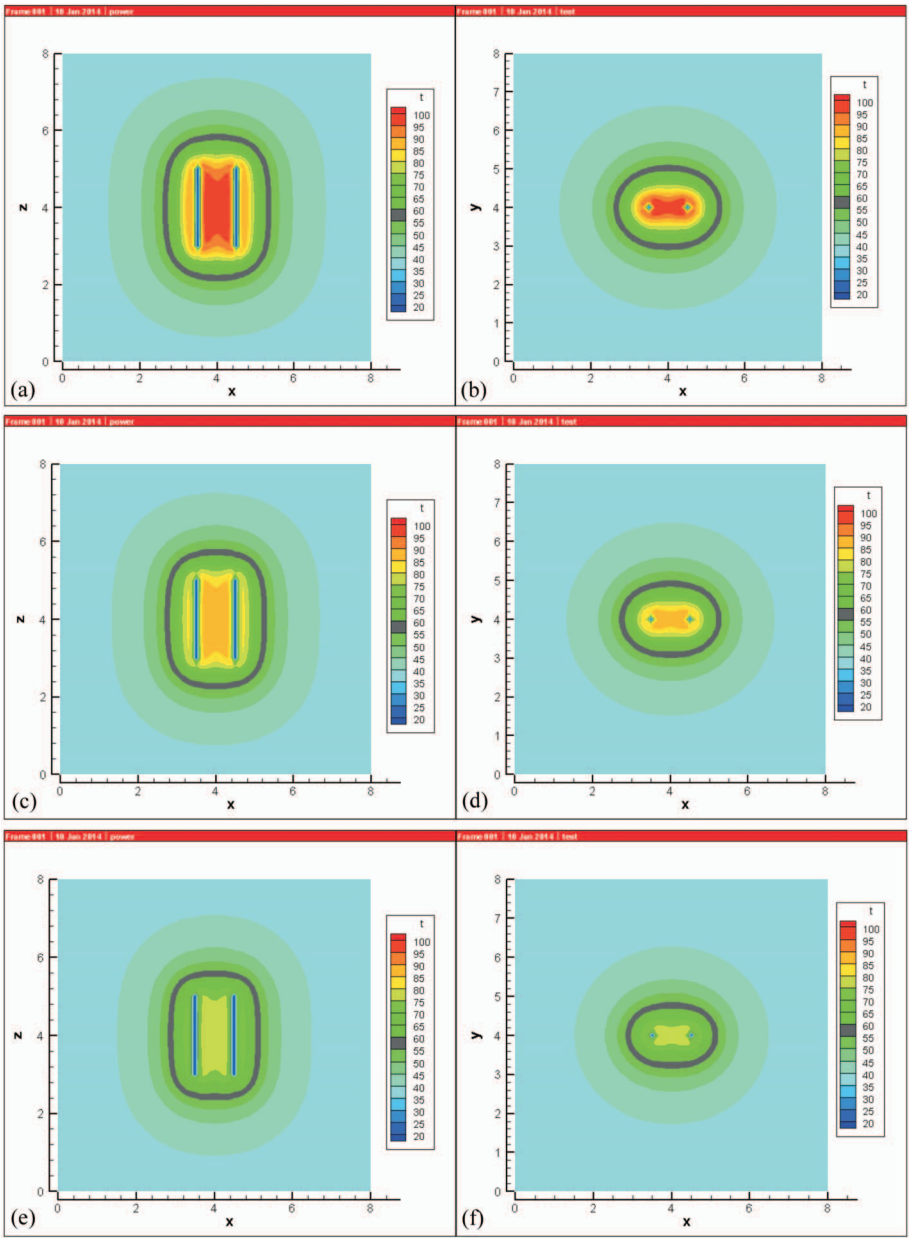

Figure 6. Temperature distributions for two-electrode radiofrequency ablation with the electrode tip exposure length of 2-cm and the electrode spacing of 1-cm at different maximum temperature (T_{max}) in the lesion.

portant impact factor during multiple-electrode clinical treatments since it affects the coagulation zone volume and may interfere with treated area's surrounding vital components in liver. Figure 7 showed RF ablation-induced coagulation zone volume generated by two parallel internally cooled electrodes which are apart at various distances in liver. In addition to 1-cm and 2-cm, several spacings have been added in Figure 7. The vertical axis value represents a ratio of coagulation zone volume by two electrdoes to that by single electrode. (i.e. 1.0 mean the thermal lesion size is identical to the lesion size generated by single internally cooled electrode only as shown in Figure 3.) Two coagulation necrosis threshold temperatures are used here: 55 °C and 60 °C. Figure 7 demonstrated that when threshold temperature is 55 °C, and the thermal lesion size could reach maximum value of 2.68, as the electrode spacing gradually increases from 0.5-cm to 2.0-cm. The value of 2.68 indicated 2.68 times the thermal lesion size generated by single internally cooled electrode during RFA. It signified that overlapping effect of heat contributions from each electrode was intensifying until reaching the maximum at the distance of 2-cm. The situation is the same when threshold temperature is 60 °C.

3.6 Three-electrode Case with Equal-distance

Rounded coagulation zone volume is normally considered an optimal design to kill tumor cells. Thus, a three-electrode case was modeled to analyze to the thermal lesion formation as shown in Figure 8. Figure 8 (a)–(j) showed temperature distributions by RFA of three internally cooled electrodes. Two electrodes (the left and right ones with spacing of 2-cm) located at the central x-z plane (i.e. y = 4-cm) as shown in Figures 8(a), (c), (e), (g) and (i) (Except for that three electrodes at the same x-z plane shown in Figure 8(a)). Figures 8(b), (d), (f), (h) and (j) are the corresponding temperature distributions at the central x-y planes (i.e. z = 4-cm), respectively. They illustrated the central electrode moving in a positive y-direction in a sequence. The sequence of figures indicated that the center electrode moved 5, 10, 15 and 18 mm up from the same baseline y = 4-cm which two other electrodes also were fixed with 2-cm apart, in a positive y-direction viewing from x-y planes (shown in Figures 8(d), (f), (h) and (j) respectively). The 18-mm indicated that the three electrodes' positions are in an equal-distance of 2-cm (with a minor location disturbance).

4. Discussions

The coagulation zone volume by multiple-electrode radiofrequency ablation (RFA) is numerically estimated based on the coagulation zone volume of single internally-cooled electrode in liver shown in Figure 3. Except rather high thermal gradient at the tip surface which was kept at below 55 °C, all other area within the T_{band} is subject to thermal lesion. The internally cooled electrode is highlighted with a segment along the z-dir shown in Figure 3(a) and a cold spot at the center is shown in Figure 3(b). A special electrode with 3-cm tip exposure and the same 1.5-mm electrode diameter (17-gauge) has been set up to compare coagulation zone volume of experimental results [14]. The mean volume in computational results is approximately 8.05 cm^3 ± 1.50 cm^3 (with T_{thresh} varied between 55 °C and 60 °C) for single internally-cooled electrode. The results showed in a good agreement with the experimental results which are 6.7 cm^3 ± 3.7 cm^3 and 7.1 cm^3 ± 3.5 cm^3 at 12- and 16- minute RF ablations [14], respectively. They indicated a steady-state approximation. In real clinic cases, typically the blood perfusion in the tumor region is lower than the surrounding normal liver tissue. The blood perfusion acts as a heat

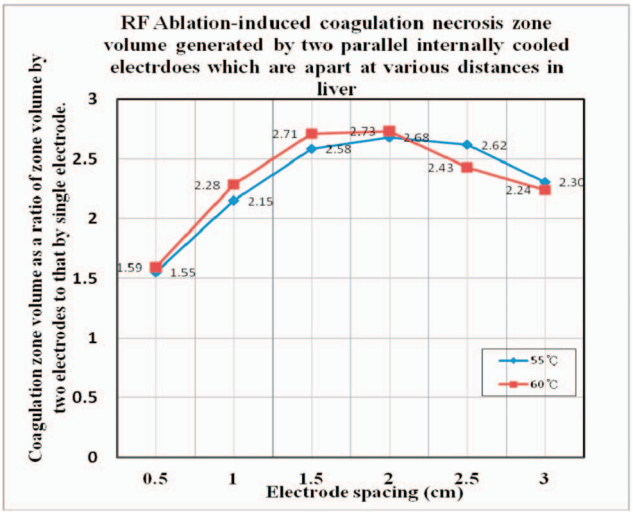

Figure 7. RF Ablation-induced coagulation zone volume generated by two parallel internally cooled electrodes which are apart at various distances in liver. The vertical axis value represents a ratio of coagulation zone volume by two electrdoes to that by single electrode. (i.e. 1.0 mean the thermal lesion size is identical to the lesion size generated by single internally cooled electrode only.) Two coagulation necrosis threshold temperatures are used here: 55 °C and 60 °C.

sink term in bio-thermal system. Thus, based on the assumption of uniform blood perfusion in computer simulation, the heating in real treatments may require less power deposition in the tumor to reach therapeutic tem-

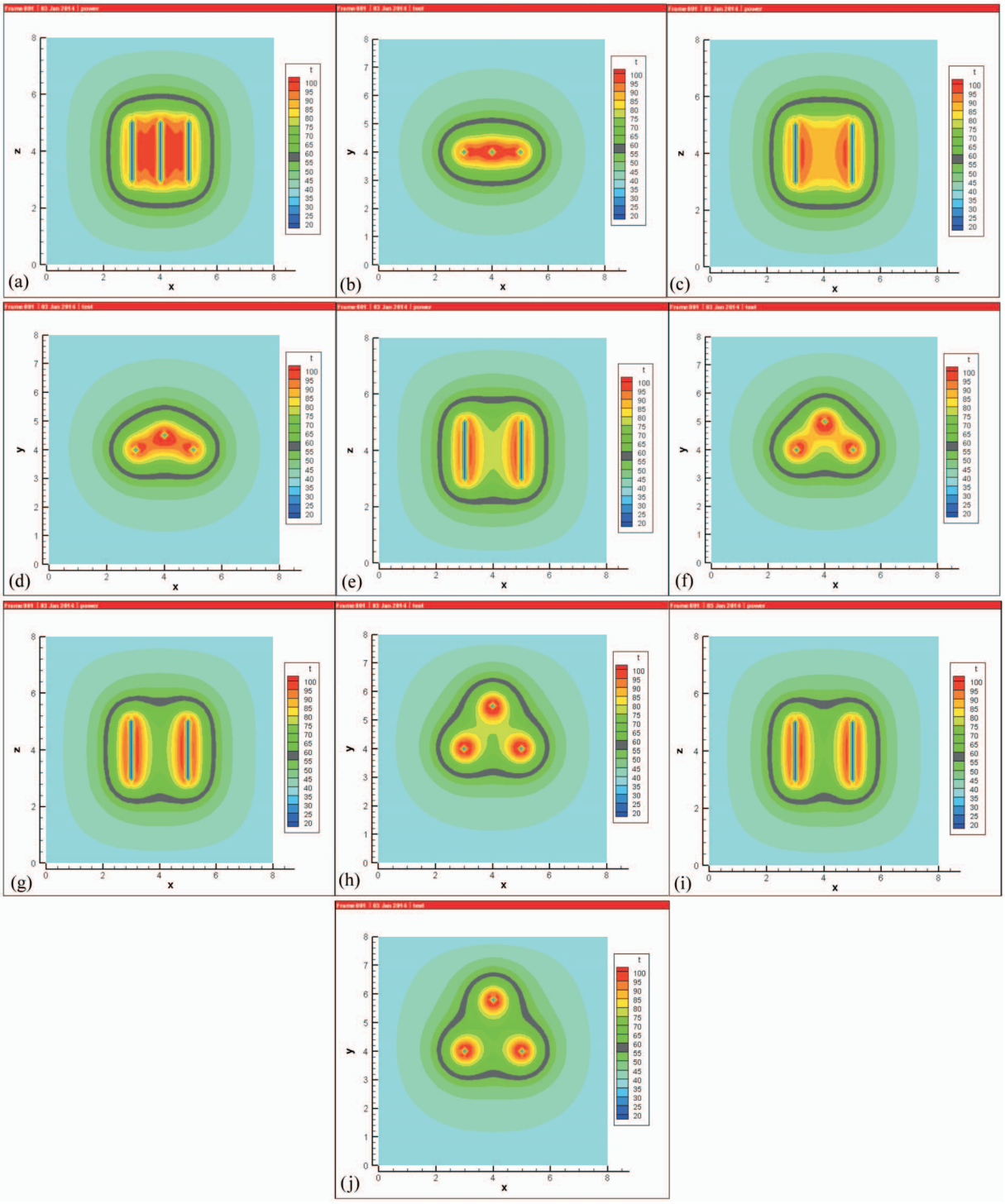

Figure 8. (a)–(j) Thermal lesion formation of three internally cooled electrodes at the central x-z planes (i.e. y = 4-cm) as shown in Figures 8(a), (c), (e), (g) and (i), and central x-y planes (i.e. z = 4-cm) as shown in Figures 8(b), (d), (f), (h) and (j). The sequence of figures indicated that the center electrode (shown in (a)) moved 5, 10, 15 and 18 mm away from the same baseline y = 4-cm (shown in (b)) which two other electrodes also resided with 2-cm apart, in a positive y-direction viewing from x-y planes (shown in Figures (d), (f), (h) and (j) respectively).

peratures as compared with the simulation cases.

Multiple-electrode structure configuration during RFA tumor treatment is a key to have large thermal lesion. The electrode spacing could change coagulation necrosis zone volume a lot as shown in Figure 4. Cleft, nonconglomerate coagulation zone that will apear as the spacing continues to increase as shown in Figures 4(a) and (b). The maximum temperature existed at the center area as a result of overlapping thermal contributions from both electrodes (shown in Figure 4(c) and (d). This could help treating tumors which are normally considerred as a sphere shape. The less concern with treating set-up configuration but indeed has significant impact on the coagulation zone volume is the electrode tip exposure length. The convex shape of thermal lesion boundary at both the top and the bottom is identical in Figures 4(c) and 5(c), except the extending longitudinal width which is due to the increment of electrode tip exposure length. However insignificant enlargement appeared in the latitudinal directions as shown in Figures 4(d) and 5(d).

RFA processing requires electrical power supply to increase lesion temperatures through electrical particles moving which generates friction. With excessive electrical power, that caused tissue temperature exceeding 100 °C and may generate vapor inside treating tissues. It then resulted in high electrical resistance and turned the system off. In normal procedure, the power is added up gradually. Patients have different treating geometry size and internal vital organs nearby the treated spot. That contributes to different levels of impact on electrical power. As the heating in parallel described in section 2.2, however if the heating is sequential, the thermal ablation results won't be the same; it has rather complicated electrical current between electrode probes and grounds. The maximum temperature in the lesion is used to express the idea of different power supply as shown in Figure 6. During clinic RFA process, powering the electrodes to treat the localized lesion area is gradually increasing. It may reach at different T_{max} due to different time, different patient's treating geometry and electrical current moving direction. Thus some variation of coagulation zone volume existed at different T_{max}. However, reaching steady-state temperatures in the lesion is rather quick (within 4~6 minutes) as pointed out from Huang [24]. This study is computational simulation for treatment planning. As to how to control the T_{max} in Figure 6 for a clinical RF ablation system, Cool-tipTM RF Ablation System E Series developed by COVIDIEN Inc. has optional remote temperature probe allows real-time tissue temperature monitoring for extra assurance. The suggested location of the temperature probe in the case of Figure 6 is placed in-between line distance of two parallel RF electrodes at the half electrode tip exposure in vertical. The precise horizontal location is close to any of two electrodes at 3-mm ± 1-mm in distance. Thus T_{max} is closely monitored and controlled.

From a simple two-electrode case, optimal coagulation zone volume is shown in Figure 7, when the electrode spacing is 2-cm. As continual increase in distance of the electrode spacing, the thermal lesion size started to decrease. It revealed heat overlapping effect no longer has futher contribution from both electrodes. In other words, less overlapping heat effect to thermal lesion volume is generated than the volume when the electrode spacing is at the distance of 2-cm. As considering threshold temperature of 60 °C, the maximum cogulation volume appeared still at the electrode spacing of 2-cm. The overlapping effect became significant when electrode spacing is less than 2-cm. However, it is significantly reducing as compared with that of threshold temperature of 55 °C when spacing is larger than 2-cm. Resulted in cleft, nonconglomerate coagulation zone that will apear as spacing continues to increase.

As to three-electrode case, similar process has been done to analyze the thermal lesion formation as shown in Figure 8. To further investigate the central electrode moving distance, Figure 9 showed the temperature distributions along the central x-direction line plot at the center x-y plane (i.e. located at z = 40-mm and y = 40-mm) with the variation of distance location of central electrode at 0, 5, 10, 15 and 18-mm within three-electrode RFA model. "0-mm" means all three-electrode are in the y = 40-mm which plot shows three-electrode temperature at water cooling temperature shown in Figures 8(a) and (b) with the central electrode located at the same baseline with the other two electrodes and "5-mm" means the central electrode moves up 5-mm in the positive y-direction. Three obvious steep thermal gradients were seen at three-electrode location at different x-directional positions. The numerical scheme is capable of calculating at those spots without divergence. The resultant coagulation necrosis cross-section shown in experiments (Figure 1 of [13]) is clover-shaped. It is consistent with the numerical calculation of equal-distance electrode spac-

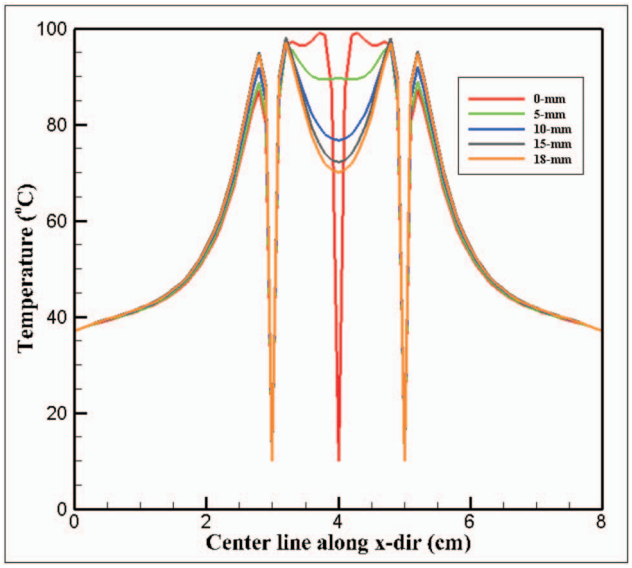

Figure 9. The temperature distributions along the central x-direction line plot at the center x-y plane (i.e. located at z = 40-mm and y = 40-mm) with the variation of distance location of central electrode at 0, 5, 10, 15 and 18-mm within three-electrode RFA model. "0-mm" means all three-electrode are in the y = 40-mm which plot shows three-electrode temperature at water cooling temperature shown in Figure (b) with the central electrode located at the same baseline with the other two electrodes and "5-mm" means the central electrode moves up 5- mm in the positive y-direction.

ing shown in Figure 8(j) with approximate 4.0-cm ± 1.0-cm in diameter. With a thermally significant blood vessel in the tumor region, cold stripe of blood vessel could be still observed in the tumor region during heating. It depends on mass flow rate and location of the blood vessel within the tumor, there may have different degree of cooling impact on tumor. As well as RF probes structure configuration which makes distance between probe and blood vessel is an important factor for treatment. This is similar to the case of single RF probe treatment with the impact of blood vessel on tumor, and details can be referred to Huang [24].

5. Conclusions

The numerical model is capable of predicting thermal lesion formation by multiple parallel internally-cooled electrodes. Results demonstrated that larger coagulation necrosis zone volume is generated with the multiple-electrode technique in minimum invasive localized RF ablation of liver tumor treatment. Overlapping thermal effect from each electrode and clover-shaped thermal lesion formation of three-electrode RFA system are highlighted in the numerical simulations which are consistent with the experimental results. The internally-cooled electrode's interface with tissue revealed extreme steep thermal gradients which are seldom calculated. And the tissue temperatures adjacent to the electrode are high, even though next to cool-tip probe during RFA processing.

Acknowledgements

The author would like to thank the Ministry of Science and Technology of Taiwan for partially supporting this research under no. NSC 102-2221-E-032 -006 and MOST 103-2221-E-032-003.

Reference

[1] Scott Gazelle, G. and Nahum Goldberg, S., "Luigi Solbiati, Tito Livraghi, Tumor Ablation with Radiofrequency Energy," *Radiology* Vol. 217, pp. 633–646 (2000). doi: 10.1148/radiology.217.3.r00dc 26633

[2] Lee, J. M., Kim, Y. K., Kim, S. W., Han, J. K., Kim, S. H. and Choi, B. I., "Combined Radiofrequency Ablation and Acetic Acid Hypertonic Saline Solution Instillation: An *In Vivo* Study of Rabbit Liver," *Korean J Radiol*, Vol. 5, pp. 31–38 (2004). doi: 10.3348/kjr.2004.5.1.31

[3] Nahum Goldberg, S., Scott Gazelle, G., Halpern, E. R., Rittman, W. J., Mueller, P. R. and Rosenthal, D. I., "Radiofrequency Tissue Ablation: Importance of Local Temperature Along the Electrode Tip Exposure in Determining Lesion Shape and Size," *Acad Radiol*, Vol. 3, pp. 212–218 (1996). doi: 10.1016/S1076-6332(96)80443-0

[4] Rosenthal, D. I., Hornicek, F. J., Torriani, M., Gebhardt, M. C. and Mankin, H. J., "Osteoid Osteoma: Percutaneous Treatment with Radiofrequency Energy," *Radiology*, Vol. 229, 171–175 (2003). doi: 10.1148/radiol.2291021053

[5] Lencioni, R. A., Allgaier, H. P., Cioni, D., et al., "Small Hepatocellular Carcinoma in Cirrhosis: Randomized Comparison of Radio-frequency Thermal Ablation Versus Percutaneous Ethanol Injection," *Radiology*, Vol. 228, pp. 235–240 (2003). doi: 10.1148/radiol.2281020718

[6] Akeboshi, M., Yamakado, K., Nakatsuka, A., et al., "Percutaneous Radiofrequency Ablation of Lung Neoplasms: Initial Therapeutic Response," *J Vasc Interv Radiol*, Vol. 15, pp. 463–470 (2004). doi: 10.1097/01.RVI.0000126812.12853.77

[7] Hwang, J. J., Walther, M. M., Pautler, S. E., et al., "Radio Frequency Ablation Of Small Renal Tumors: Intermediate Results," *J Urol*, Vol. 171, pp. 1814–1818 (2004). doi: 10.1097/01.ju.0000119905.72574.de

[8] Lin, S.-M., "Local Ablation for Hepatocellular Carcinoma in Taiwan," *Liver Cancer*, Vol. 2, pp. 73–83 (2013). doi: 10.1159/000315237

[9] Kosari, K., Gomes, M., Hunter, D., Hess, D. J., Greeno, E. and Sielaff, T. D., "Local, Intrahepatic and Systemic Recurrence Patterns after Radiofrequency Ablation of Hepatic Malignancies," *J Gastrointest Surg*, Vol. 6, pp. 255–263 (2002). doi: 10.1016/S1091-255X(02)00002-1

[10] Kuvshinoff, B. W. and Ota, D. M., "Radiofrequency Ablation of Liver Tumors: Influence of Technique and Tumor Size," *Surgery*, Vol. 132, pp. 605–611 (2002). doi: 10.1067/msy.2002.127545

[11] Dodd, G. D. 3rd, Frank, M. S., Aribandi, M., Chopra, S. and Chintapalli, K. N., "Radiofrequency Thermal Ablation: Computer Analysis of the Size of the Thermal Injury Created by Overlapping Ablations," *AJR*, Vol. 177, pp. 777–782 (2001). doi: 10.2214/ajr.177.4.1770777

[12] Laeseke, P. F., Frey, T. M., Brace, C. L., Sampson, L. A., Winter, T. C., Ketzler, J. R. and Lee, F. T., "Multiple-electrode Radiofrequency Ablation of Hepatic Malignancies: Initial Clinical Experience," *AJR, Am. J. Roentgenol*, Vol. 188, pp. 1485–1494 (2007). doi: 10.2214/AJR.06.1004

[13] Goldberg, S. N., Solbiati, L., Hahn, P. F., et al., Large-volume Tissue Ablation with Radio Frequency by Using a Clustered, Internally Cooled Electrode Technique: Laboratory and Clinical Experience in Liver Metastases," *Radiology*, Vol. 209, pp. 371–379 (1998). doi: 10.1148/radiology.209.2.9807561

[14] Laeseke, P. F., Sampson, L. A., Haemmerich, D., Brace, C. L., Fine, J. P., Frey, T. M., Winter III, T. C., Lee, F. T., "Multiple-Electrode Radiofrequency Ablation Creates Confluent Areas of Necrosis: In Vivo Porcine Liver Results," *Radiology*, Vol. 241, No. 1, pp. 116–124 (2006). doi: 10.1148/radiol.2411051271

[15] Solazzo, S. A., Liu, Z., Lobo, S. M., Ahmed, M., Hines-Peralta, A. U., Lenkinski, R. E. and Goldberg, S. N., "Radiofrequency Ablation: Importance of Background Tissue Electrical Conductivity – an Agar Phantom and Computer Modeling Study," *Radiology*, Vol. 236, pp. 495–502 (2005). doi: 10.1148/radiol.2362040965

[16] Lobo, S. M., Liu, Z. J., Yu, N. C., Humphries, S., Ahmed, M., Cosman, E. R., Lenkinski, R. E., Goldberg, W. and Goldberg, S. N., "RF Tumour Ablation: Computer Simulation and Mathematical Modelling of the Effects of Electrical and Thermal Conductivity," *Int J Hyperthermia*, Vol. 21, pp. 199–213 (2005). doi: 10.1080/02656730400001108

[17] Haemmerich, D., Staelin, T., Tungjitkusolmun, S., Lee, Jr., F. T., Mahvi, D. M. and Webster, J. G., "Hepatic Bipolar Radio-Frequency Ablation between Separated Multiprong Electrodes," *IEEE Transactions On Biomedical Engineering*, Vol. 48, No. 10 (2001). doi: 10.1109/10.951517

[18] Labonte, S., "A Computer Simulation of Radio-frequency Ablation of the Endocardium," *IEEE Trans Biomed Eng*, Vol. 41, pp. 883–890 (1994). doi: 10.1109/10.312096

[19] Labonte, S., "Numerical Model for Radio-frequency Ablation of the Endocardium and its Experimental Validation," *IEEE Trans Biomed Eng*, Vol. 41, pp. 108–115 (1994). doi: 10.1109/10.284921

[20] Vahid Shahidi, A. and Savard, P., "A Finite Element Model for Radiofrequency Ablation of the Myocardium," *IEEE Transactions On Biomedical Engineering*, Vol. 41, No. 10 (1994). doi: 10.1109/10.324528

[21] Scheinman, Ed., M. M., *Catheter Ablation* of *Cardiac Arrhythmias*, Boston: Martinus Nijhoff Publ. (1988).

[22] Chang, I. A. and Nguyen, U. D., "Thermal Modeling of Lesion Growth with Radiofrequency Ablation Devices," *Biomed Eng Online*, Vol. 3, p. 27 (2004). doi: 10.1109/TBME.2004.827545

[23] Chang, I., "Finite Element Analysis of Hepatic Radiofrequency Ablation Probes Using Temperature- Dependent Electrical Conductivity," *Biomed Eng Online*, Vol. 2, p. 12 (2003).

[24] Huang, H.-W., "Influence of Blood Vessel on the Thermal Lesion Formation during Radiofrequency Ablation for Liver Tumors," *Med. Phys*., Vol. 40, No. 7, (2013). doi: 10.1118/1.4811135

[25] Huang, H.-W., Liauh, C.-T., Chou, C.-Y., Shih, T.-C. and Lin, W.-L., "A Fast Adaptive Power Scheme Based on Temperature Distribution and Convergence Value

for Optimal Hyperthermia Treatment," *Appl. Therm. Eng*., Vol. 37, pp. 103–111 (2012). doi: 10.1016/j.applthermaleng.2011.11.003

[26] Huang, H.-W., Liauh, C.-T., Horng, T.-L., Shih, T.-C., Chiang, C.-F. and Lin, W.-L., "Effective Heating for Tumors with Thermally Significant Blood Vessels during Hyperthermia Treatment," *Appl. Therm. Eng*., Vol. 50, pp. 837–847 (2013). doi: 10.1016/j.applthermaleng.2012.07.018

[27] Tungjitkusolmun, S., Woo, E. J., Cao, H., Tsai, J.-Z., Vorperian, V. R. and Webster, J. G., "Finite Element Analyses of Uniform Current Density Electrodes for Radio-frequency Cardiac Ablation," *IEEE Trans. Biomed. Eng*., Vol. 47, No. 1, pp. 32–40 (2000). doi: 10.1109/10.817617

[28] "Cool-tipTM RF Ablation System," Retrieved 21 May (2013) (Available URL: http://www.cool-tiprf.com/4minute.html).

[29] Lobo, S. M., Afzal, K. S., Ahmed, M., Kruskal, J. B., Lenkinski, R. E. and Goldberg, S. N., "Radiofrequency Ablation: Modeling the Enhanced Temperature Response to Adjuvant NaCl Pretreatment," *Radiology*, Vol. 230, pp. 175–182 (2004). doi: 10.1148/radiol.2301021512

[30] McGahan, J. P. and Dodd, III, G. D., "Radiofrequency Ablation of Liver Tumors: Current Status," *AJR, Am. J. Roentgenol*., Vol. 176, pp. 3–16 (2001). doi: 10.2214/ajr.176.1.1760003

[31] Goldberg, S. N., Gazelle, G. S. and Mueller, P. R., "Thermal Ablation Therapy for Focal Malignancy: A Unified Approach to Underlying Principles, Techniques and Diagnostic Imaging Guidance," *AJR, Am. J. Roentgenol*., Vol. 174, pp. 323–331 (2000). doi: 10.2214/ajr.174.2.1740323

[32] Lapidus, L. and Pinder, G. F., Numerical Solution of Partial Differential Equations in Science and Engineering (Wiley-Interscience, New York) (1982).

[33] Chen, Z.-P., Roemer, R. B. and Cetas, T. C., "Three-dimensional Simulations of Ferromagnetic Implant Hyperthermia," *Med. Phys*., Vol. 19, No. 4, pp. 989–997 (1992). doi: 10.1118/1.596787

[34] Huang, H. W., "Simulation of Large Vessels in Hyperthermia Therapy," M. S. Thesis, University of Arizona, Tucson, AZ (1992).

[35] Chen, Z. P., "A Three-dimensional Treatment Planning Program for Hyperthermia," Ph.D. Dissertation, University of Arizona, Tucson, AZ (1989).

[36] Huang, H.-W., Roemer, R. B. and Chen, Z. P., "A Counter Current Vascular Network Model of Heat Transfer in Tissues," *ASME J. Biomech. Eng*., Vol. 118, pp. 120–129 (1996). doi: 10.1115/1.2795937

[37] Haemmerich, D. G., "Finite Element Modeling of Hepatic Radio Frequency Ablation," Ph.D. Dissertation, University of Wisconsin, Madison (2001). doi: 10.1109/TBME.2002.800790

[38] Ebbini, E. S., Umemura, S.-I., Ibbini, M. and Cain, C. A., "A Cylindricalsection Ultrasound Phased-array Applicator for Hyperthermia Cancer Therapy," *IEEE Trans. Biomed. Eng*., Vol. 35, pp. 561–572 (1988). doi: 10.1109/58.8034

Manuscript Received: ???
Accepted: ???